Characterization of the planar differential mobility analyzer (DMA P5)：resolving power, transmission efficiency and its application to atmospheric cluster measurements

Zhengning Xu[1], Jian Gao[1], Zhuanghao Xu[1], Michel Attoui[3], Xiangyu Pei[1], Mario Amo-González[4], Kewei Zhang[1], Zhibin Wang[1,2*]

[1]Zhejiang Provincial Key Laboratory of Organic Pollution Process and Control, MOE Key Laboratory of Environment Remediation and Ecological Health, College of Environmental and Resource Sciences, Zhejiang University, Hangzhou 310058, China
[2]ZJU-Hangzhou Global Scientific and Technological Innovation Center, Zhejiang University, Hangzhou 311215, China
[3]University Paris-Est Creteil, University Paris-Diderot, LISA, UMR CNRS 7583, France
[4]MION S.L., Avda. Francisco Valles 8, Boecillo, Valladolid, 47151, Spain

Correspondence to: Zhibin Wang (wangzhibin@zju.edu.cn)

Abstract. The newly developed planar differential mobility analyzer (DMA) serving as particle sizer can achieve higher transmission and selection precision at ambient pressure compared with conventional cylindrical DMA, and show potentials on coupling with atmospheric pressure interface mass spectrometer (API-MS) for cluster detection with an additional ion mobility dimension. In this study, we assessed the performance of a commercial planar DMA (DMA P5) integrated with the home-build recirculation system. The sizing range of the system in this work is 0-3.9 nm, although larger sizes can be measured with a sheath gas flow restrictor. The resolving power under different recirculation setups (suction mode and counter flow mode) and different sheath flow rates was evaluated using electrosprayed tetra-alkyl ammonium salts (TMAI, TBAI, THAB and TDAB). The maximum resolving power of THA$^+$ under suction and counterflow mode are 61.6 and 84.6, respectively. The sizing resolution of DMA P5 is 7-16 times higher than conventional cylindrical DMAs. The resolving power showed approximately linear correlation with $\sqrt{V_{DMA}}$ under counterflow mode, while the resolving power of THA$^+$ under suction mode stopped linearly increase with $\sqrt{V_{DMA}}$ when the V_{DMA} was above 3554.3V and enter a plateau due to the interference of sample flow on the laminarity of sheath flow. The transmission efficiency of DMA P5 can reach 54.3%, about one factor of magnitude higher than the commercial DMAs. The mobility spectrum of different electrosprayed tetra-alkyl ammonium salts and the mass to charge ratio-mobility 2D spectrum of sulfuric acid clusters was also characterized with the DMA P5 (-MS) system.

1 Introduction

Measurement of the physical and chemical properties of sub-3 nm particles is essential for understanding atmospheric aerosol nucleation mechanisms (Kerminen et al. 2018). Differential mobility analyzer (DMA) has long been used for aerosol sizing and classifying (Knutson & Whitby, 1975). TSI Nano-DMA (Model 3085, Chen et al., 1998) and TSI 1 nm-DMA (Model

3086, Stolzenburg et al., 2018) were designed for particle sizing down to 3 nm and 1 nm, respectively. Equipped with these DMAs, the newly developed DEG-based scanning mobility particle sizer (SMPS) system (Jiang et al., 2011) can be applied to measure the size distributions of sub-3 nm particles (Cai et al., 2017).

Various mass spectrometry-based approaches have been utilized for measuring the chemical composition of clusters and their precursors (Chen et al., 2020; Peng et al., 2022). However, these approaches lack direct measurement of cluster size and structure. In Thermal Desorption Chemical Ionization Mass Spectrometer (TDCIMS) system (Smith et al., 2004), size resolved particles were separated by DMA(s), and analyzed by mass spectrometry when sufficient particles were accumulated thorough electrostatic deposition. Currently, the detect limit of TDCIMS was 5 nm (Perraud et al., 2020). For cluster study, a much longer accumulation period is needed, due to the drastic decrease of charging efficiency with decreased particle diameter and low ion transmission of the applied DMAs. DMAs coupled directly to mass spectrometer (DMA-MS) can achieve spontaneous detection of ion mobility and chemical composition, and can serve as a promising tool to study the physicochemical properties of atmospheric clusters and the formation mechanism of particle nucleation and initial growth (Zhang et al., 2022). The performance of the applied DMA on sizing sub-3 nm particles is the only limitation of this technique.

Planar DMAs have been successfully coupled to several commercial atmospheric pressure interface mass spectrometer (API-MS) under high resolving power and high transmission (Hogan and Fernandez de la Mora, 2009; 2010; Hogan et al., 2011; Criado-Hidalgo et al., 2013). The physicochemical properties of various atmospheric clusters such as metal iodide clusters (Oberreit et al., 2014; Oberreit et al., 2015), dimethylamine (DMA) and sulfuric acid complexes (Ouyang et al., 2015; Thomas et al., 2016), sodium chloride clusters (Li and Hogan, 2017) and hybrid iodine pentoxide–iodic acid clusters (Ahonen et al., 2019) were investigated by DMA-MS. Rus et al. (2010) have characterized several prototypes of planar DMAs and the transmission of DMA P4 was ~50%. On the basis of DMA P4, DMA P5 updated the design of outlet, guaranteeing that the assemble/disassemble of DMA to/from MS would not break the vacuum (Amo-González and Pérez, 2018).

To our knowledge, the characterization of commercial DMA P5 have not been reported. In this work, the performance of DMA P5 under different working conditions with a home-build recirculation circuit was characterized. The resolving power and transmission efficiency were characterized using standard ion clusters. The DMA P5 was also deployed to measure the ion mobility spectrum of electrosprayed clusters of different tetra-alkyl ammonium salts and the mass to charge ratio-ion mobility 2D spectrum of sulfuric acid.

2 Experimental setup and methodology

In this study, DMA P5 (SEADM, Valladolid, Spain) was used, which consisted of a pair of plate parallel electrodes separated by insulated holders. The combination of horizontal laminar sheath flow and vertical electric field between the separation region of the two electrodes acts a spatial mobility filter (Purves et al., 1998). Polydispersed aerosols penetrating through inlet slit at the inlet electrode move toward the outlet electrode under the electric field force. For a fixed sheath flow velocity and electric field pair, monodispersed aerosols with super narrow ion mobility range can penetrate through the outlet hole at the

Atmospheric
Measurement
Techniques
Discussions

Open Access

EGU

outlet electrode and transmit to the detectors. The detailed design and critical dimensions of DMA P5 has been described by Amo-González and Pérez (2018). The theoretical principle of planar DMA on particle sizing is described in SI (Section 1).

65 The ion mobility of selection can be estimated by the following the formula:

$$Z = \frac{U \cdot h^2}{L \cdot V_{DMA}} \qquad (1)$$

where Z represents the ion mobility of selection, U represents the velocity of sheath flow, h represents the distance of the two electrodes, L represents the horizontal distance between inlet slit and outlet hole, V_{DMA} represents the voltage difference between the two electrodes.

70 The home-made recirculation circuit was adapted, providing particle free sheath flow with stable velocity and temperature. The recirculation circuit consist of air blower (Ref 497.3.265-361, Domel), home-build water cooler coupled with constant temperature water bath (DCW-2008, SCIENTZ), particle filter (Ref 34230010, Megalem MD143P3, Camfil Farr) adapted for high flow velocity, NW40 and NW 50 corrugated stainless-steel tubes and connectors. The rotational speed of the blower was controlled by 0-10 Vdc analogue signal (V_{blower}). The flow rate under different control voltage was calculated by Eq. (1) using

75 the ion mobility and VDMA of standard ion (THA$^+$) (Fig.S2). The temperature was controlled to be 24 Celsius degrees.

The nano-ESI ionization source (SEADM, Valladolid, Spain) was adapted. The main body of the nano-ESI ionization source is a PEEK cubic electrospray chamber, assembled with the inlet electrode of DMA P5 on its bottom, sealed on front and back ends by two glass windows, coupled with 1/8" capillary guide on the top middle. There were another two 1/4" ports for flow injection and exhaust on the top left and right of the ionization chamber.

80 In this study, two types of recirculation circuit setup (suction mode and counter flow mode) were characterized based on the design of ionization source. Under suction mode, aerosols were transport to the inlet slit by the combination of the electric field between the electrospray and the DMA inlet electrode and the polydisersed aerosol flow (Q_{in}) and sucked into the separation region under the monodispersed aerosol flow (Q_{out}), the excess flow (Q_{excess}) was exhausted from another port. Under counter flow mode, only one port was used to exhaust the counter flow (Q_{count}) out of the inlet slit. Compensate flow

85 (Q_c), with the flow rate equal to the sum of Q_{count} and Q_{out}, was introduced into the circuit thorough a T connector. The detailed recirculation circuit setups are illustrated in Fig. 1.
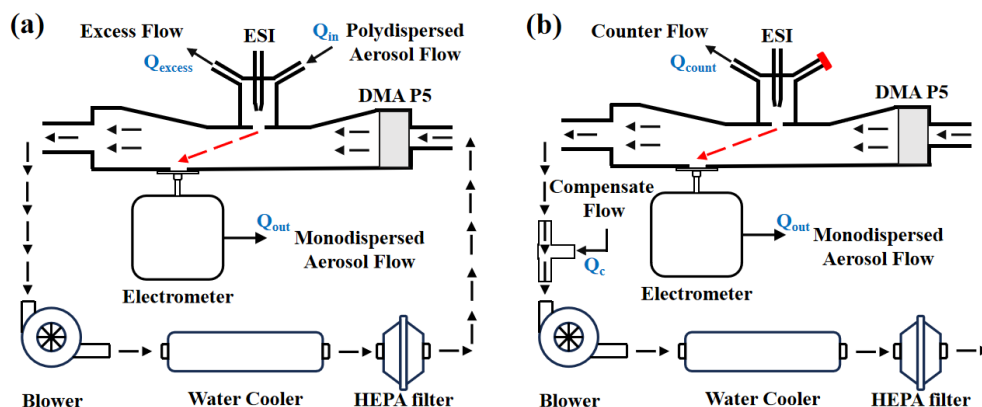
Fig.1 Schematic diagram of the recirculation circuit setups (a) suction mode; (b) counter flow mode of DMA P5 system.

The performance of the DMA P5 was characterized by classifying aerosols generated via electrospraying of salt solutions. A
90   silica capillary (FS360-50-N-5-C50, New Objective) fitted in the capillary guide of nano-ESI ionization source was applied to
connect the ionization chamber and the vial of solution. The connections on both ends of the capillary were established with
standard capillary connections used for liquid chromatography. The vial was connected to a pressure sensor and a syringe
equipped with a valve thorough a T-connector. The solution was pushed through the capillary by compressing the gas inside
the vial until the desired pressure above the solution surface was achieved. The valve in front of the springer was then turned
95   off, keeping the pressure constant for a long period. High voltage was applied to the solution through an inert metal wire
immersed in it. Similar methodologies have been proposed by Jiang et al. (2011) and Cai et al. (2018). With positive voltage
applied and without subsequent neutralization, singly charged, positive polarity aerosols can be generated (Ude and Fernández
de la Mora 2005). In this study, pressure (P_{ES}) and voltage (V_{ES}) of the electrospray source were set to ~20 kPa and ~2000 V,
respectively. The Faraday cage electrometer (Lynx E11, SEADM, Valladolid, Spain, Fernandez de la Mora et al., 2017) was
100   used as particle counter. Based on Eq. (1), the ion mobility of any aerosols with known DMA voltage can be calibrated with
standard ions under constant sheath flow velocity by the following formula:

$$Z = \frac{V_{standard} * Z_{standard}}{V_{DMA}} \qquad (2)$$

where $Z_{standard}$ represents the electric mobility of standard ion, V_{DMA} and $V_{standard}$ represent the DMA voltage of target aerosol
and standard ion under the same sheath flow rate. Standard ion (THA⁺), with the known mobility of 0.97 cm^2 V^{-1} s^{-1} (Ude and
105   Fernández de la Mora 2005), was generated via positive electrospraying of 0.5 mM THABr solution in 9:1 methanol/water
mixture. The mobility diameter in this manuscript is calculated with the Stokes-Cunningham equation (Tammet, 1995;
Wiedensohler et al., 2012). Detailed information about the mobility diameter calculation is described in SI (Section 2). The
sizing range under different rotational speed was calculated using Eq. (2), given the upper VDMA limit of 10 kV. The sizing
upper limit of DMA P5 in the current configuration was 1.9-3.9 nm, although using a flow restrictor in the sheath gas circuit
110   the upper size can be extended. Higher sheath flow rate corresponded to lower sizing range (Fig. S2).

The sizing resolution of specific aerosol (R) is defined as the ratio of the central electrical mobility (Z) and the full width at half maximum for the peak (ΔZ_{FWHM}) (Flagan 1999):

$$R = \frac{Z}{\Delta Z_{FWHM}} \quad (3)$$

The theoretical calculation of planar DMA sizing resolution is given by the following equation (Amo-González and Pérez, 2018):

$$R^{-1} = \frac{\Delta L_{0.5}}{L} = \sqrt{\left[\left(\frac{Q_{in}+Q_{out}}{L_{slit} 2\, Re\, v}\right)^2 + \frac{16 ln2 kT}{V_{DMA} N_e}\left(1 + \left[\frac{h}{L}\right]^2\right)\right]} \quad (4)$$

where, Q_{in} represent the polydispersed aerosol flow rate and Q_{out} is the monodispersed aerosol flow rate, respectively, L_{slit} is the length of inlet slit, Re is the Reynolds number, v is the viscosity of the sheath gas, k is the Boltzmann's constant, T is the absolute temperature of the sheath gas, Ne is the net charge on the aerosol.

3 Results and Discussion

3.1 Resolving Power under different recirculation modes

The voltage applied to the nano-ESI source floats above the inlet electrode voltage of DMA P5. Such configuration can avoid the influence of the voltage change during the scanning mode on the formation and stability of electrospray. Moreover, the electric field between the capillary tip and the inlet electrode guides the aerosol into the DMA separation chamber. According to such design, as being illustrated in the former section, two recirculation modes can be applied for DMA P5 operation. Under suction mode, polydispersed aerosols are sucked into the DMA separation region. Under counter flow mode, the aerosols are inserted electrically into the DMA, the inlet slit counter flow accelerates the evaporation of droplets and prevent the neutral droplets from entering the DMA separation region.

Based on Eq. (4), large Re is expected in order to achieve high sizing resolution, under which condition the sheath flow velocity needs to be very large based on the following equation:

$$Re = \frac{Uh}{v} \quad (5)$$

Suction of aerosol sample can easily disturb the sheath flow, and decrease the sizing resolution. Moreover, incomplete desolvation of solvent and entrance of neutral droplet into the DMA separation region under suction mode may also affect the peak shape, obscuring the identification of analytes of interest (Amo-González and Fernández de la Mora, 2017). On the other hand, suction mode can obtain higher aerosol number concentration at the expense of resolving power and peak shape.

Atmospheric
Measurement
Techniques
Discussions
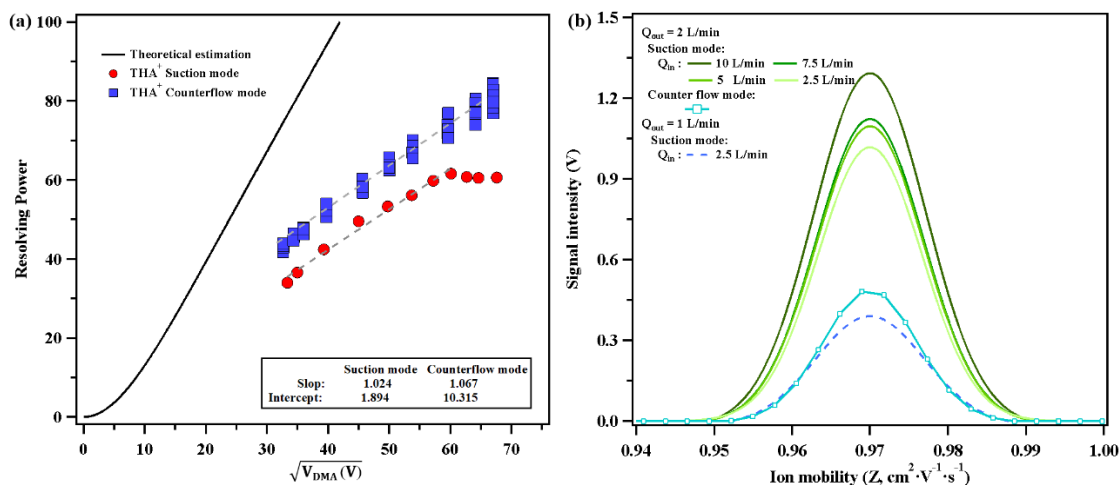
Fig 2. (a) The dependency of the resolving power of THA$^+$ on DMA voltage (V_{DMA}) under suction mode and counter flow mode; (b) dependency of the resolving power and signal intensity on the Q_{out} under suction mode and the comparison with counterflow mode.

According to Eq. (1), V_{DMA} is approximately linearly correlated with the sheath gas velocity under fixed ion mobility.

140   According to Eq. (4), R increases with the increase of $\sqrt{V_{DMA}}$ with determined DMA physical structure (h, L), sheath flow properties (v, T, U) and aerosol charge state (Ne). Figure 2a shows the dependency of the resolving power of sizing 1.47 nm ions (THA$^+$) on $\sqrt{V_{DMA}}$ under two recirculation modes by changing the sheath flow velocity. Q_{out} is 2 L/min under the two recirculation modes. Q_{in} is 5 L/min under suction mode. $Q_{counter}$ is 0.5 L/min under counter flow mode.

Under suction mode, R showed positive linear correlation with $\sqrt{V_{DMA}}$, with the slope and intercept of 1.024 and 1.894,

145   respectively, when the V_{DMA} was below 3554.3V. R remained nearly unchanged with the increase of $\sqrt{V_{DMA}}$, when the V_{DMA} was above 3554.3V. In high V_{DMA} range (corresponding to higher sheath flow velocity), R was in the range of 60 ± 3. Under counter flow mode, R and $\sqrt{V_{DMA}}$ showed good linear relationship (R^2=0.95) within the sheath flow velocity range of the applied system. The slope and intercept of 1.067 and 10.315, respectively.

Generally, the resolving power of THA$^+$ was higher under counter flow mode, and was much closer to the theoretical

150   calculation. With the increase of the sheath flow velocity, the difference between the measurement and the theoretical calculation gradually increased. Under the suction mode, due to the interference of polydispersed sample flow, the resolving power was 14.9%-21.7% lower than that of the counter flow mode when $\sqrt{V_{DMA}}$ was lower than 59.6. The discrepancy increased to 24.9 % when $\sqrt{V_{DMA}}$ reached 66.0. The reason for the difference of resolving power between the two recirculation modes and the deviation from the theoretical calculation is the turbulence effect. The higher the sheath flow rate velocity is,

155   the easier for the flow to become turbulent, consistent with the measurement result that the resolving power stopped increasing when V_{DMA} was over 3554.3V. The increasing discrepancy of measured and theoretical resolving power was attributed to the insufficient stabilization of sheath flow to the laminar condition. Adding an additional pair of prelaminarizer screens into the

sheath flow recirculation circuit under counter flow mode can increase the resolving power approaching it to the theoretical limit (Amo-González and Pérez, 2018).

160   Figure 2b shows the change of THA$^+$ peak signal intensity and resolving power to different Q_{in} under suction mode. The change of Q_{in} showed little effect on resolving power (58.06-61.58, with the relative deviation being -3.5%-2.3%), while had significant influence on signal intensity (number concentration of the sizing aerosol). With constant Q_{out} of 2 L/min, the peak signal of THA$^+$ is 1.31 V, 1.13 V, 1.1 V and 1.02 V, under Q_{in} of 10 L/min, 7.5 L/min, 5 L/min and 2.5 L/min, respectively. When Q_{out} was decreased to 1.0 L/min, the signal strength was significantly reduced. It should also be noted that at the cost of

165   the decreased resolving power, higher signal intensity of electrometer was obtained under suction mode. The peak signal of THA$^+$ under suction mode was 108.2%-167.3% higher compared with counter flow mode at the same Q_{out}.

Under the counter flow mode, there are two adjustable parameters, namely counter flow rate (Q_{count}), and monodispersed aerosol flow rate (Q_{out}). Figure 3 shows the influence of Q_{count} and Q_{out} on the sizing resolution and number concentration under the fixed sheath flow rate (about 1200 L/min, under which speed the recirculation system can operate for a long time

170   without increase of temperature). Figure 3a and b show the change of THA$^+$ central voltage and signal intensity under different Q_{out} at Q_{count} of 0.5 L/min and 1.0 L/min, respectively. In general, the signal strength increased monotonously with the increase of Q_{out}. According to theory (Knutson & Whitby, 1975), the THA$^+$ central voltage decreased with the increase of Q_{out}. Compared with Q_{count}, Q_{out} had a greater impact on the measurement results. Figure 3c shows the relationship of the integrated peak area of THA$^+$, the resolving power and the central voltage with Q_{out}. With the increase of Q_{out} from 0.5 L/min to 3.0

175   L/min, the central voltage of THA$^+$ decreased by about 20 V (less than 1%); the integrated peak area increased by 7.6 and 6.8 times for Q_{count} of 1.0 L/min and 0.5 L/min, respectively; the resolving power decreased from 75 to 69. We defined the counting efficiency of electrometer as the integrated peak area / Q_{out}. The relation of the counting efficiency with Q_{out} (Fig. S3) indicated that the counting efficiency would increase with the increase of Q_{out} before reaching 2 L/min and decrease afterward. Setting the total Q_{out} over 2.0 L/min would result in the decreasing of both counting efficiency and resolving power and is not

180   recommended when coupling with an API-MS.
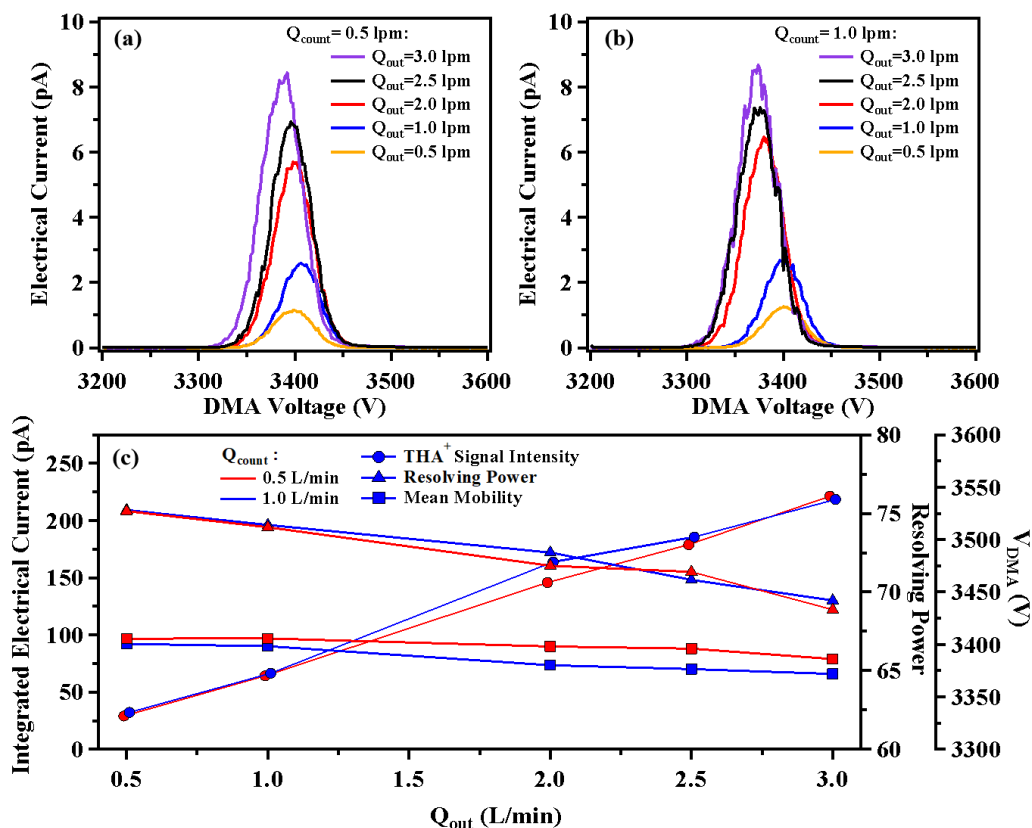
Fig. 3 Mobility spectrum of THA$^+$ under different Q_{out} with (a) $Q_{counter}$ = 0.5 L/min; (b) $Q_{counter}$ = 1.0 L/min; (c) Integrated signal intensity, resolving power and V$_{DMA}$ of THA$^+$ under different Q_{out}.

The sizing resolution of THA$^+$ by DMA P5 and Half Mini (Fernandez de la Mora and Kozlowski, 2013) were compared with the results of different types of commercial DMAs (Jiang et al., 2011). The comparison results show that the planar DMA has the highest sizing resolution, which is 7-16 times higher than conventional cylindrical DMAs and 5-6 times higher than Half Mini (Fig. 4). The mobility spectrum of THA$^+$ obtained from Half Mini is shown in Fig. S4. The obtained well separated THA$^+$ ion beam was utilized for characterizing the ion transmission efficiency of DMA P5.
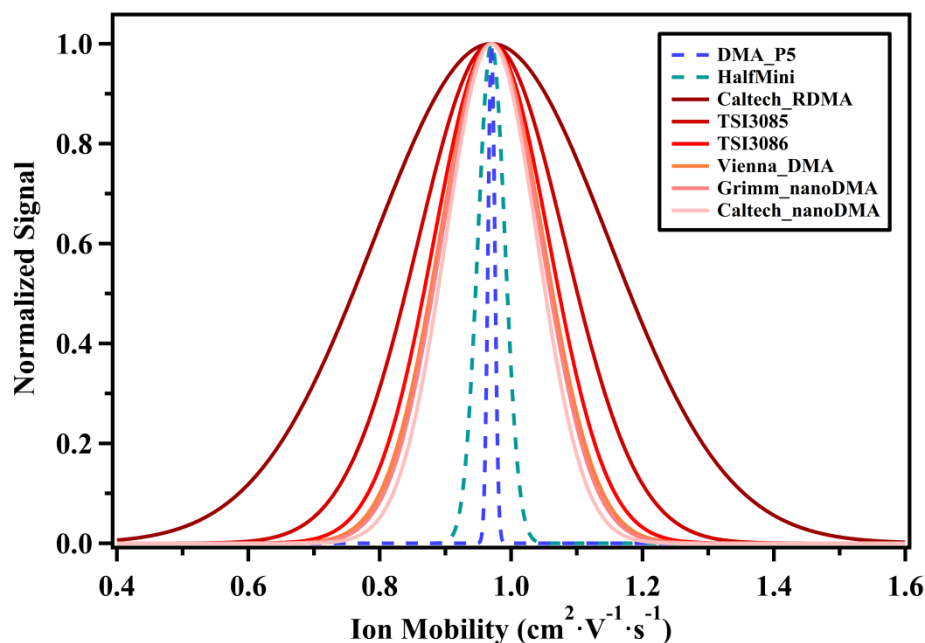
Fig. 4 Comparison of the resolving power of DMA P5 and other commercial DMAs for detecting THA⁺. DMA P5 was operated under the sheath flow rate of 1500 L/min, Half Mini was operated under the sheath flow rate of 300 L/min.

3.2 Transmission efficiency

Transmission efficiency is defined as the ratio of particle number passing thorough the DMA to particle number at the DMA inlet. The transmission efficiency of DMA P5 was characterized using a tandem DMA system (Fig. S5). Standard aerosol ions (THA⁺) were generated following the same method described above. A Half Mini DMA operated at fixed sheath flow and voltage was applied as the upstream DMA selecting only THA⁺ monomer. Such configuration can minimize the influence of multi-charged ions with larger molecular weights (Attoui et al., 2013). To verify that the upstream DMA carried only THA⁺ monomer, before each experiment, a full mobility spectrum was taken under voltage scanning mode and compared with published result (Liu et al., 2021). Lynx E11 and E12, with amplifications of 1×10^{11} and 1×10^{12} V/A, respectively, were used to measure the aerosol number concentration upstream and downstream of the DMA P5. An additional experiment connecting the two electrometers to the Half Mini DMA thorough a flow splitter (TSI 3780) with the same tube length was conducted to determine the correction factor. The Half Mini DMA was operated under fixed voltage, selecting only THA⁺ ions. The sample flow rates of the electrometers were measured using a bubble flowmeter. The signal of the two electrometers was measured simultaneously. The correction factor of the two electrometers was 10.34, which it is quite close to the theoretical amplification relation of the two electrometers. In order to correct the ion loss to the tube wall, the tube length between the flow splitter (TSI 3780) and the electrometers (excluding the DMA P5) were identical. Ion transmission efficiency was equal to the ratio between the ion number concentrations measured by the downstream and upstream electrometer, both given by the following equation:

$$N = V_{EM}/(amp \cdot e \cdot q) \qquad (6)$$

9

where V_{EM} represent the signal of electrometer, *amp* is the amplification coefficient of the electrometer, q is the sample flow

210 rate of electrometer and e represents elementary charge.

DMA P5 was operated under suction mode with inlet electrode grounded, and outlet electrode connected to the negative voltage. The grounded downstream electrometer was connected to outlet electrode with a straight 10 cm dissipative plastic tube (85A, FreelinWade, Oregon) (Attoui et al., 2016). Counter flow mode was not tested due to the difficulty to control the electric field needed for conventional positive voltage setting (inlet electrode connected to positive voltage, and outlet electrode

215 grounded) to push the ions against the counter flow with the presence of the sample tube. These experiments were carried out under different sheath flow velocity (corresponding to different control voltage, Fig. S2). The transmission efficiency as the function of Q_{out} are shown in Fig. 5a. The transmission efficiency showed linearly correlation with increased Q_{out}. The highest ion transmission was 54.3% under the highest Q_{out} (3 L/min) and the lowest sheath flow velocity. Under the above-mentioned configuration, electric field between outlet electrode with a high negative voltage and the grounded electrometer will drag

220 THA$^+$ ions back to the DMA outlet constantly. Sufficient Q_{in} is called to compensate the electrical velocity. As depicted by Eq (1), higher V_{DMA} is needed for selecting particle with the same mobility under higher sheath flow velocity. With increasing sheath flow velocity, the ion transmission efficiency decreased due to insufficient compensation of electrical velocity. It should be noted that under conventional DMA P5 configuration (both outlet electrode and detectors are grounded), the ion loss due to the electrical dragging force is negligible. Thus, the transmission efficiency is no longer related to the Q_{out}. Consequently,

225 our results represented the lower limit of the DMA P5 ion transmission. The ion transmission of TSI 1 nm-DMA (Model 3086) was also characterized with the same TDMA system. The ion transmission was 4.7% and 7.1% for sheath/ sample flow ratio of 25 L/min /2.5 L/min and 30 L/min / 3.0 L/min, respectively. DMA P5 illustrated 4.5-17.5 times higher ion transmission efficiency compared with other cylindrical DMAs (Fig. 5b).
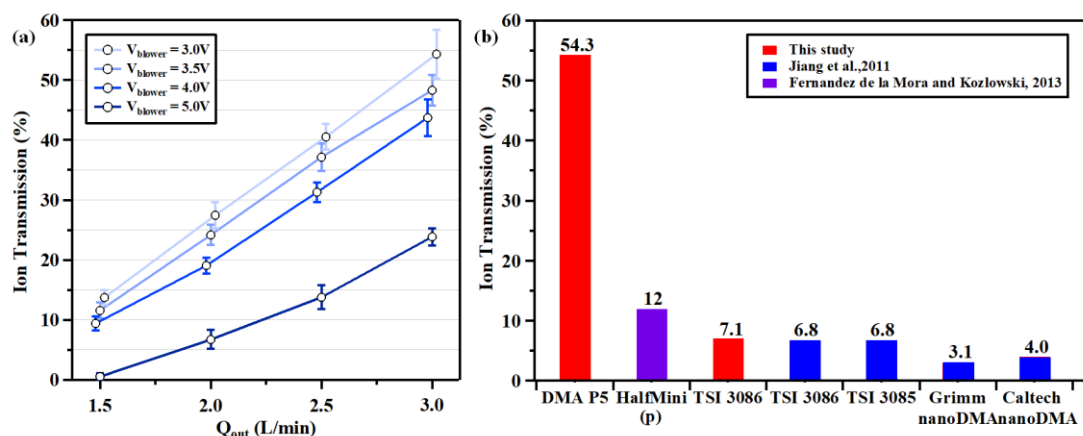
230 **Fig. 5 (a) Ion transmission efficiency of P5 under different Q_{out}; (b) Comparison with other cylindrical DMAs (the red bars represent the experimental results).**

3.3 Applications on aerosol sizing and coupling with mass spectrometer

In addition to THAB, the sizing ability of DMA P5 was also characterized with three other tetra alkyl ammonium halides (tetra methyl ammonium iodide (TMAI), tetra butyl ammonium iodide (TBAI) and tetra decyl ammonium bromide (TDAB)).

235 The concentration of the solution is 0.5 mM/L. Figure 6 and Figure 7 show the positive and negative ion mobility spectra. The results showed that well defined, single positive charged monomers and dimers can be obtained for the four salt solutions, trimers of TBAI and THAB can also be observed. The negative ions of halogen elements are the main products in the negative ion spectrum. Eq. (2) is used to calculate the mobilities of aerosol ions, and the results are shown in Table S1 and Table S2. The estimated results were consistent with the results reported by Ude et al. (2005).
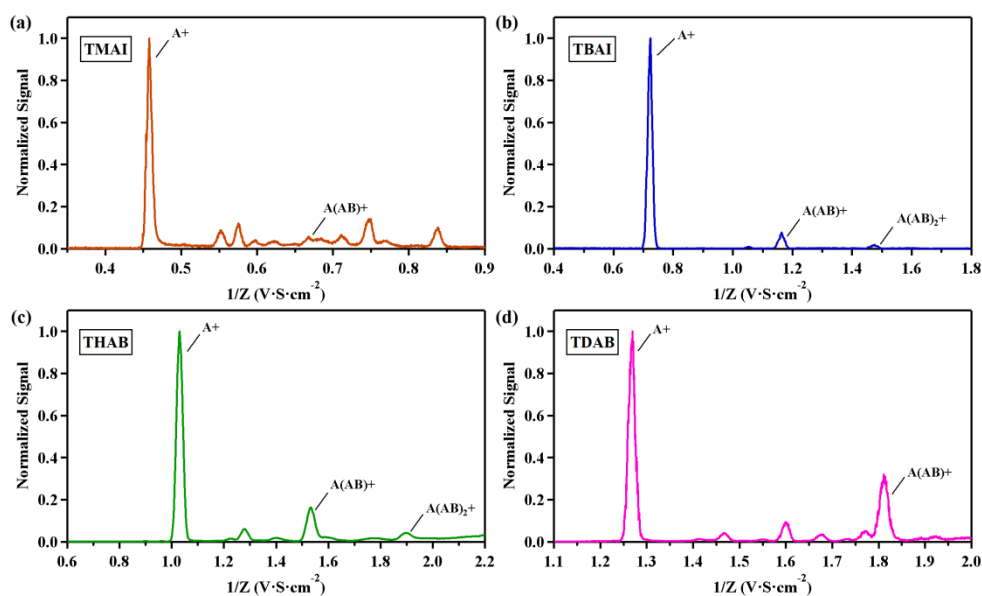
240

Fig. 6 Positive mobility spectrum of electrosprayed tetra-alkyl ammonium ions, (a) TMAI, (b) TBAI, (c) THAB, (d) TDAB.
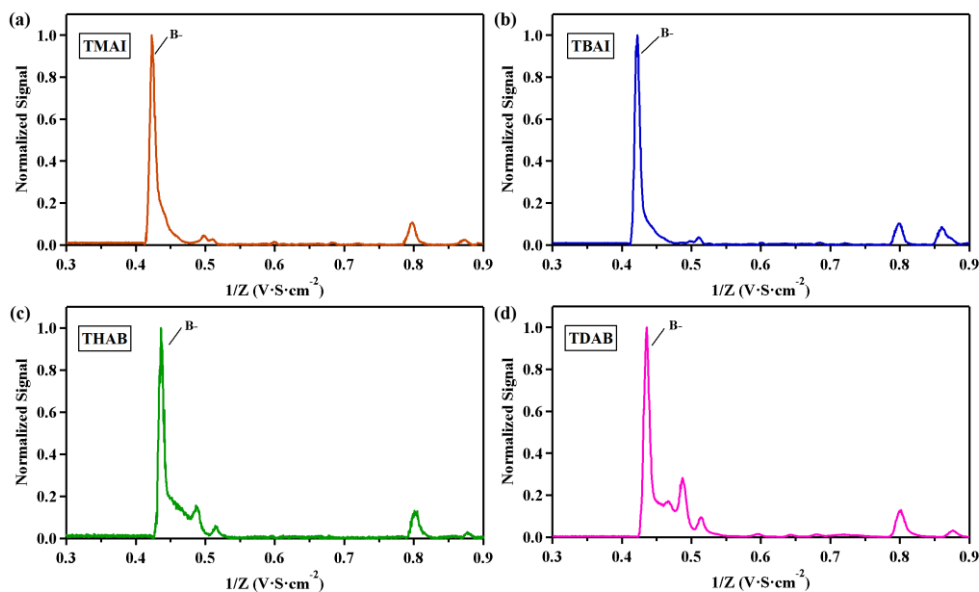
Fig. 7 Negative mobility spectrum of electrosprayed tetra-alkyl ammonium ions, (a) TMAI, (b) TBAI, (c) THAB, (d) TDAB.

According to equation Eq. (4), the resolving power of planar DMA is directly related to V_{DMA} and Ne. The relationship between

245   the resolving power of the positive charged monomers of THAB, TMAI, TBAI and TDAB with the V_{DMA} under different

sheath flow velocity is shown in Figure 8. The result showed that the resolving power (R) and $\sqrt{V_{DMA}}$ of different types of

tetra alkyl ammonium cations presented an excellent linear relationship ($R^2=0.96$), with the slope and intercept of 0.992 and

13.511. As illustrated in Fig. 8, most data points were within the 95% confidence interval. This result can be used as the

resolution function for multi-peak fitting, and it can be applied in peak identification of multi-component complexes. The

250   resolution function of multiple charged ions should also be established in the further.

Atmospheric
Measurement
Techniques
Discussions
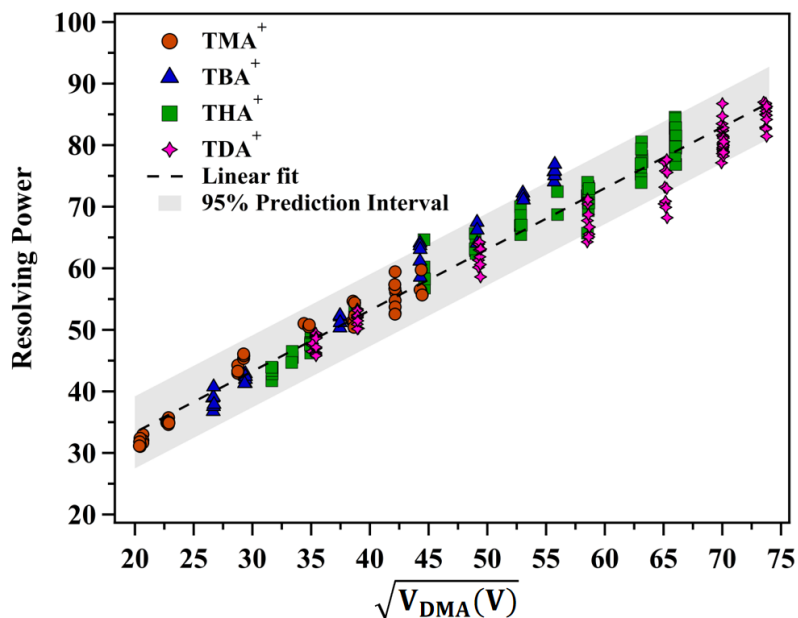
Fig. 8 Relation of resolving power of different cluster ions with V_{DMA}

Sulfuric acid molecules and clusters, as important participants of new particle formation (Kulmala et al., 2000), were chosen to evaluate the performance of DMA P5 as an ion mobility filter for the study of atmospheric clusters. The experimental set-

255 up consisted of the nano-ESI ionization source, connected to the DMA P5. The exit of the DMA P5 was connected to a Lynx E11 electrometer and to an API-ToF-MS (TOFWERK AG, Switzerland), thorough a customized interface (MION, Valladolid, Spain). 200 mM sulfuric acid solution in 1:4 methanol/water mixture was used to generate negatively charged sulfuric acid clusters by ESI. The generation procedure was the same as the former sections. The mobility of sulfuric acid clusters was calibrated before each experiment with THA$^+$. Hereafter the bisulfate ions (HSO$_4^-$), negatively charged sulfuric acid dimers

260 (H$_2$SO$_4$HSO$_4^-$), trimers ((H$_2$SO$_4$)$_2$HSO$_4^-$) and tetramers ((H$_2$SO$_4$)$_3$HSO$_4^-$) are referred as sulfuric acid monomer (SA)$_1^-$, dimer (SA)$_2^-$, trimer (SA)$_3^-$ and tetramer (SA)$_4^-$, respectively.

Table 1 mobilities 1/Z (V s^{-1}cm^{-2}) and diameter (nm) of sulfuric acid clusters

Peak$^+$	1/Z	Diameter
(SA)$_1^-$	0.497	1.02
(SA)$_2^-$	0.502	1.024
(SA)$_3^-$	0.589	1.111
(SA)$_4^-$	0.676	1.191

The ion mobility spectrum and ion mobility-mass to charge ratio 2D distribution (DMA-MS spectrum) are shown in Fig 9.

265 The multi-peak fitting analysis of the ion mobility spectrum was conducted with Igor. The fitted peaks were then identified

Atmospheric
Measurement
Techniques
Discussions

Open Access

EGU

with the DMA-MS spectrum. Well separated $(SA)_3^-$ and $(SA)_4^-$ peaks were observed. Due to insufficient resolution, $(SA)_1^-$ and $(SA)_2^-$ were not separated within the ion mobility spectrum. The ion mobility (diameter) of $(SA)_1^-$ and $(SA)_2^-$ were obtained thorough DMA-MS spectrum. Table 1 shows the ion mobility and diameter of sulfuric acid monomer and larger clusters. The measured diameter of $(SA)_3^-$ was 1.11 nm, showed high consistency with the reported value (Passananti et al., 2019). Since

270 the voltage configurations can affect the fragmentation of the cluster inside the API-ToF-MS (Passananti et al., 2019), the DMA-MS spectrum is highly instrument dependent. Cautions should be paid on the comparison between different experiments.
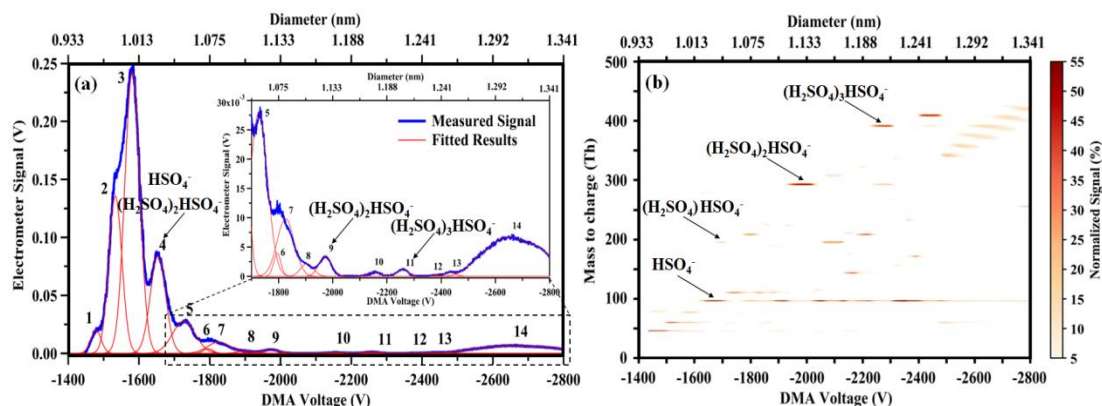
Fig. 9 Negative ion mobility spectrum of electrosprayed sulfuric acid of (a) electrometer and (b) DMA P5 coupled to API-ToF-MS.

4 Conclusions and Recommendations

275 We present the characterization results of a planar DMA (DMA P5) with a home-made recirculation system. With this recirculation system, the sizing range of DMA P5 is 0-3.9 nm. Two operation modes can be applied (suction mode and counter flow mode). Under suction mode, the maximum resolving power can reach 60, while under counter flow mode, the maximum resolving power is 84, much closer to the theoretical limit. The resolving power of DMA P5 is 7-16 times higher than commercial DMAs. Under suction mode, the obtained monodispersed aerosol number concentration can be modified by

280 changing the injection flow rate. Under counter flow mode, although the resolving power is higher than the suction mode, the obtained monodispersed aerosol number concentration is lower due to the absence of injection flow. The ion transmission of DMA P5, tested by a TDMA system, exceeds 54.3%, which is about 7-8 times higher than commercial DMA (TSI 3086). The application of DMA P5 was also characterized. Positive and negative aerosol ions of four tetra alkyl ammonium halides (THAB, TMAI, TBAI and TDAB) were measured, and high-resolution ion spectra were obtained. Finally, P5 was combined

285 with an API-TOF-MS to successfully measure the two-dimensional (mass to charge ratio V.S. ion mobility) distribution of sulfuric acid clusters. The mobility diameters of sulfuric acid clusters (monomer to tetramer) were measured.

This system can be used to simultaneously measure the ion mobility and chemical composition of atmospheric clusters. In addition, this system can also be applied to calibrate the mass dependent ion transmission efficiency of mass spectrometry and

study the impact of the collision induced cluster fragmentation (CICF) inside the mass spectrometry on the measurement

290 results of atmospheric clusters.

Data Availability

Data available on request from the authors.

Conflicts of Interest

The authors declare no conflict of interests.

295 Author Contributions

Zhengning Xu: Methodology, System set up, Experiment, Formal analysis, Visualization, Writing Original draft, Review and editing. **Jian Gao, Zhuanghao Xu:** Experiment, System set up and Data curation. **Michel Attoui, Xiangyu Pei:** System set up, Review and editing. **Mario Amo-González, Kewei Zhang:** System set up. **Zhibin Wang:** Conceptualization, Project administration, Review and editing; Funding acquisition.

300 Acknowledgments

References

305 Ahonen, L., Li, C., Kubecka, J., Iyer, S., Vehkamaki, H., Petaja, T., Kulmala, M., and Hogan, C. J.: Ion mobility-mass spectrometry of iodine pentoxide-iodic acid hybrid cluster Anions in dry and humidified atmospheres, J. Phys. Chem. Lett. 10 (8), 1935–1941, https://doi.org/10.1021/acs.jpclett.9b00453, 2019.

Amo-González, M. and Pérez, S.: Planar Differential Mobility Analyzer with a Resolving Power of 110, Analytical Chemistry, 90, 6735-6741, 2018.

310 Amo- González, M., and Fernández de la Mora, J.: Mobility peak tailing reduction in a differential mobility analyzer (DMA) coupled with a mass spectrometer and several ionization sources, J. Am. Soc. Mass Spectrom. 28 (8),1506–1517, https://doi.org/10.1007/s13361-017-1630-2, 2017.

Attoui, M., M. Paragano, J. Cuevas, and J. Fernandez de la Mora.: Tandem DMA generation of strictly monomobile 1–3.5nm particle standards, Aerosol Sci. Technol. 47 (5):499–511, 2013.

315 Attoui, M. and Fernandez de la Mora, J.: Flow driven transmission of charged particles against an axial field in antistatic tubes at the sample outlet of a Differential Mobility Analyzer, Journal of Aerosol Science, 100, 91-96, 2016.

Cai, R.; Chen, D.-R.; Hao, J.; Jiang, J.: A miniature cylindrical differential mobility analyzer for sub-3 nm particle sizing, Journal of Aerosol Science, 106, 111-119, 2017.

Cai, R.; Attoui, M.; Jiang, J.; Korhonen, F.; Hao, J.; Petäjä, T.; Kangasluoma, J.: Characterization of a high-resolution

320 supercritical differential mobility analyzer at reduced flow rates, Aerosol Science and Technology, 52, (11), 1332-1343, 2018.

Chen, D.-R., Pui, D. Y. H., Hummes, D., Fissan, H., Quant, F. R., and Sem, G. J.: Design and Evaluation of a Nanometer Aerosol Differential Mobility Analyzer (Nano-DMA), J. Aerosol Sci., 29(5):497–509. http://doi.org/10.1016/S0021-8502(97)10018-0, 1998.

Chen, Y., Wang, W., Liu, M., and Ge, M.: Measurement technologies of nanoparticle chemical composition and their

325 application, J. Atmos. Environ. Opt. 15 (6), 402–412 , http://doi.org/10.3969/j.issn.1673-6141.2020.06.001,2020

Criado-Hidalgo, E., Fernandez-Garcia, J., and Fernandez de la Mora, J.: Mass and charge distribution analysis in negative electrosprays of large polyethylene glycol chains by ion mobility mass spectrometry, Anal. Chem. 85 (5), 2710–2716, http://doi.org/10.1021/ac303054x, 2013.

Fernández de la Mora, J., and Kozlowski, J.: Handheld differential mobility analyzers of high resolution for 1–30nm particles:

330 Design and fabrication considerations, J. Aerosol Sci. 57:45–53, 2013.

Fernández de la Mora, J., Perez-Lorenzo, L. J., Arranz, G., Amo- González, M., and Burtscher, H.: Fast high-resolution nanoDMA measurements with a 25 ms response time electrometer, Aerosol Sci. Technol., 51, (6), 724-734, 2017.

Flagan, R. C.: On differential mobility analyzer resolution, Aerosol Sci. Technol. 30 (6):556–70, 1999.

Hogan, C. J., Jr., and Fernandez de la Mora, J.: Tandem ion mobility mass spectrometry (IMS-MS) study of ion evaporation

335 from ionic liquidacetonitrile nanodrops, Phys. Chem. Chem. Phys. 11 (36), 8079–8090, http://doi.org/10.1039/b904022f, 2009.

Hogan, C. J., Jr., and Fernandez de la Mora, J.: Ion-pair evaporation from ionic liquid clusters, J. Am. Soc. Mass Spectrom. 21 (8), 1382–1386, http://doi.org/10.1016/j.jasms.2010.03.044, 2010.

Hogan, C. J., Jr., Ruotolo, B. T., Robinson, C. V., and Fernandez de la Mora, J.: Tandem differential mobility analysis-mass spectrometry reveals partial gas-phase collapse of the GroEL complex, J. Phys. Chem. B 115 (13), 3614–3621,

340 http://doi.org/10.1021/jp109172k, 2011.

Jiang, J., Chen, M., Kuang, C., Attoui, M., & McMurry, P. H.: Electrical mobility spectrometer using a diethylene glycol condensation particle counter for measurement of aerosol size distributions down to 1 nm, Aerosol Science and Technology, 45, 510–521, 2011.

Jiang, J., Attoui, M., Heim, M., Brunelli, N. A., McMurry, P. H., Kasper, G., Flagan, R. C., Giapis, K., and Mouret, G.: Transfer

345 Functions and Penetrations of Five Differential Mobility Analyzers for Sub-2 nm Particle Classification, Aerosol Science and Technology, 45, (4), 480-492, 2011.

Kerminen, V.-M., Chen, X., Vakkari, V., Petäjä, T., Kulmala, M. and Biachi, F.: Atmospheric new particle formation and growth: review of field observations, Environ. Res. Lett., http://doi.org/10.1088/1748-9326/aadf3c, 2018.

Knutson, E. O., & Whitby, K. T.: Aerosol classification by electric mobility: Apparatus, theory, and applications, Aerosol
350   Science and Technology, 6, 443–451, 1975.

Kulmala, M., Pirjola, L., Mäkelä, J. M.: Stable sulphate clusters as a source of new atmospheric particles, Nature, 404, (6773), 66-69, 2000.

Li, C. X., and Hogan, C. J.: Vapor specific extents of uptake by nanometer scale charged particles. Aerosol Sci. Technol. 51 (5), 653–664, http://doi.org/10.1080/02786826.2017.1288285, 2017.

355   Liu, Y., Attoui, M., Chen, J., Li, Q. and Wang, L.: Performance comparison of SMPSs with soft X-ray and Kr-85 neutralizers in a humid atmosphere, Journal of Aerosol Science, 154, 2021.

Oberreit, D., Rawat, V. K., Larriba-Andaluz, C., Ouyang, H., McMurry, P. H., and Hogan, C. J.: Analysis of heterogeneous water vapor uptake by metal iodide cluster ions via differential mobility analysis-mass spectrometry, J. Chem. Phys. 143 (10), 104204. http://doi.org/10.1063/1.4930278, 2015.

360   Oberreit, D. R., McMurry, P. H., and Hogan, C. J.: Analysis of heterogeneous uptake by nanoparticles via differential mobility analysis-drift tube ion mobility spectrometry, Phys. Chem. Chem. Phys. 16 (15), 6968–6979, http://doi.org/10.1039/c3cp54842b, 2014

Ouyang, H., He, S., Larriba-Andaluz, C., and Hogan, C. J.: IMS-MS and IMS-IMS investigation of the structure and stability of dimethylamine-sulfuric acid nanoclusters, J. Phys. Chem. A 119 (10), 2026–2036, http://doi.org/10.1021/jp512645g, 2015.

365   Passananti, M., Zapadinsky, E., Zanca, T., Kangasluoma, J., Myllys, N., Rissanen, M. P., Kurten, T., Ehn, M., Attoui, M., Vehkamaki, H.: How well can we predict cluster fragmentation inside a mass spectrometer? Chem Commun (Camb), 55, (42), 5946-5949, 2019.

Peng, C., Deng, C., Lei, T., Zheng, J., Zhao, J., Wang, D., Wu, Z., Wang, L., Chen, Y., Liu, M, Jiang, J., Ye, A., Ge, M., Wang, W.: Measurement of atmospheric nanoparticles: Bridging the gap between gas-phase molecules and larger particles, J. Environ.
370   Sci, http://doi.org/10.1016/j.jes.2022.03.006, 2022.

Perraud, V., Li, X. X., Jiang, J. K., Finlayson-Pitts, B. J., and Smith, J. N.: Size-resolved chemical composition of sub-20 nm particles from methanesulfonic acid reactions with methylamine and ammonia, ACS Earth Space Chem. 4 (7), 1182–1194, http://doi.org/10.1021/acsearthspacechem.0c00120, 2020.

Purves, R. W., Guevremont, R., Day, S., Pipich, C. W., and Matyjaszczyk, M. S.: Mass spectrometric characterization of a
375   high-field asymmetric waveform ion mobility spectrometer, Rev. Sci. Instrum., 69, 4094−4104, http://doi.org/10.1063/1.1149255, 1998.

Rus, J., Moro, D., Sillero, J. A., Royuela, J., Casado, A., Estevez-Molinero, F., and Fernández de la Mora, J.: IMS–MS studies based on coupling a differential mobility analyzer (DMA) to commercial API–MS systems. Int. J. Mass Spectrom. 298 (1), 30–40, http://doi.org/10.1016/j.ijms.2010.05.008, 2010.

380   Smith, J. N., Moore, K. F., McMurry, P. H., and Eisele, F. L.: Atmospheric measurements of sub-20 nm diameter particle chemical composition by thermal desorption chemical ionization mass spectrometry, Aerosol Sci. Technol. 38 (2), 100–110, http://doi.org/10.1080/02786820490249036, 2004.

Stolzenburg, M., Scheckman, J., Attoui, M., Han, H., and McMurry, P.: Characterization of the TSI model 3086 differential mobility analyzer for classifying aerosols down to 1 nm, Aerosol Science and Technology, 52:7, 748-756,

385   http://doi.org/10.1080/02786826.2018.1456649, 2018.

Tammet, H.: SIZE AND MOBILITY OF NANOMETER PARTICLES, CLUSTERS AND IONS, J. Aerosol Sci., 6, (3), 459-475, https://doi.org/10.1016/0021-8502(94)00121-E, 1995.

Thomas, J. M., He, S., Larriba-Andaluz, C., DePalma, J.W., Johnston, M. V., and Hogan, C. J.: Ion mobility spectrometry-mass spectrometry examination of the structures, stabilities, and extents of hydration of dimethylamine-sulfuric acid clusters,

390   Phys. Chem. Chem. Phys., 18, (33), 22962–22972, http://doi.org/10.1039/c6cp03432b, 2016.

Ude, S. and Fernández de la Mora, J.: Molecular monodisperse mobility and mass standards from electrosprays of tetra-alkyl ammonium halides, J. Aerosol Sci., 36, (10), 1224-1237, 2005.

Wiedensohler, A., Birmili, W., Nowak, A., Sonntag, A., Weinhold, K., Merkel, M., et al.: Mobility particle size spectrometers: harmonization of technical standards and data structure to facilitate high quality long-term observations of atmospheric particle

395   number size distributions, Atmos. Meas. Tech., 5, (3), 657-685, 2012.

Zhang, K., Xu, Z., Gao, J., Xu, Z., and Wang, Z.: Review of online measurement techniques for chemical composition of atmospheric clusters and sub-20nm particles, Frontiers in Environmental Science, 10, 2022.